



Noble gas diffusivity hindered by low energy sites in amphibole

Colin R.M. Jackson^{a,*}, David L. Shuster^{b,c}, Stephen W. Parman^d, Andrew J. Smye^e

^a *Geophysical Laboratory, Carnegie Institution of Washington, 5251 Broad Branch Road NW, Washington, DC 20015-9801, USA*

^b *Department of Earth and Planetary Science, University of California, Berkeley, 479 McCone Hall, Berkeley, CA 94720-4767, USA*

^c *Berkeley Geochronology Center, 2455 Ridge Road, Berkeley, CA 94709, USA*

^d *Department of Earth, Environment, and Planetary Sciences, Brown University, 324 Brook Street, Providence, RI 02912, USA*

^e *Department of Earth Sciences, University of Oxford, South Parks Road, Oxford OX1 3AN, UK*

Received 28 June 2015; accepted in revised form 22 September 2015; Available online 28 September 2015

Abstract

The diffusion kinetics of He and Ne in four amphibole specimens have been experimentally determined using stepwise degassing analysis of samples previously irradiated with energetic protons, and Arrhenius relationships have been fit to these data. The primary finding is that He and Ne diffusivities are systematically lower in amphiboles that have higher concentrations of unoccupied ring sites, suggesting that unoccupied ring sites act as traps for migrating noble gases. Ring site influence of noble gas diffusivity in amphiboles has substantial implications for $^{40}\text{Ar}/^{39}\text{Ar}$ thermochronology applied to these phases and the efficiency of noble gas recycling in subduction zones. These findings are consistent with the correlation between noble gas solubility and the concentration of unoccupied ring sites in amphibole (Jackson et al., 2013a, 2015) but are inconsistent with the ionic porosity model for noble gas diffusion (Fortier and Giletti, 1989; Dahl, 1996). Rather, these findings suggest that the topology of ionic porosity and absolute volume of ionic porosity compete in determining the rate at which noble gases diffuse.

© 2015 Elsevier Ltd. All rights reserved.

1. INTRODUCTION

Much of our understanding of noble gas diffusion in amphibole is motivated by its utility to thermochronology. Harrison (1981) conducted hydrothermal experiments where Ar was extracted from hornblende and pargasite samples under controlled temperatures and durations. The data from both minerals define an Arrhenius relationship that has become the standard for estimating Ar closure temperatures (T_c , Dodson, 1973) for amphiboles, independent of composition. The uniform adoption of a single Arrhenius relationship for a mineral as chemically diverse as amphibole, however, has been questioned (e.g., O'Nions et al., 1969; Berry and McDougall, 1986; von

Blanckenburg and Villa, 1988; Dahl, 1996). For example, it has been shown that chemically distinct amphiboles from single host rocks or single outcrops also have distinct $^{40}\text{Ar}/^{39}\text{Ar}$ ages, presumably related to their differing retention of Ar along a common cooling trajectory (Harrison and Fitzgerald, 1986; Onstott and Peacock, 1987; Dahl, 1996). From these observations, geochemical parameters, such as Fe# ($\text{Fe}/(\text{Fe} + \text{Mg})$, atomic), have been suggested to control the mobility of noble gases in amphibole. The recognition of strong compositional control on Ar diffusivity hinders applications of amphibole $^{40}\text{Ar}/^{39}\text{Ar}$ thermochronometry without knowledge of sample-specific kinetics and more general predictions of noble gas retentivity in amphibole during subduction.

The rate of noble gas diffusion in amphibole affects the interpretation of $^{40}\text{Ar}/^{39}\text{Ar}$ measurements and the efficiency of noble gas subduction. For $^{40}\text{Ar}/^{39}\text{Ar}$ measurements, applicable Arrhenius relationships are required to calculate

* Corresponding author. Tel.: +1 858 531 8544.

E-mail address: cjackson@ciw.edu (C.R.M. Jackson).

closure temperatures for amphibole and to place $^{40}\text{Ar}/^{39}\text{Ar}$ data in a metamorphic or magmatic context (e.g., [Harrison and McDougall, 1980](#); [Zeitler, 1985](#); [Hacker and Wang, 1995](#)). While for subduction, it is key to quantify the diffusivity of noble gases in amphibole and other major hydrothermal phases so that the rate of noble gas exchange between minerals and fluids can be calculated along slab geotherms. When combined with measurements of noble gas solubility, these data for hydrothermal phases can be used to model the distribution of noble gases between fluids and minerals during in slab environments, ultimately allowing for the prediction of recycling efficiency and elemental fractionations of noble gases associated with subduction zones.

Compositional controls on noble gas diffusion in amphibole have been modeled using the concept of ionic porosity ([Fortier and Giletti, 1989](#); [Dahl, 1996](#)). Ionic porosity is the fraction of the unit cell not occupied by ions; essentially the amount of ‘free space’ between the atoms in a mineral. The basis for this model is the broad correlation between diffusivity of O and Ar and ionic porosity for a range of silicates, including amphibole ([Dowty, 1980](#); [Fortier and Giletti, 1989](#)). The range in ionic porosity for natural amphiboles is large ($\sim 3.5\%$), reflecting the extreme compositional diversity within the amphibole family ([Dahl, 1996](#)). The largest factor controlling the range of ionic porosity within the amphibole family is related to the A-site, or ring site. The ring site is a large radius site that can be completely occupied by large radius cations (Na and K) in endmembers such as richterite and pargasite or completely unoccupied in endmembers such as actinolite or glaucophane. This exchange alone accounts for a large proportion of the total range in ionic porosity within the amphibole family. For example, between the endmembers edenite and hornblende *sensu stricto* exchange of octahedral Mg and ring site-hosted Na with octahedral Al and an unoccupied ring site accounts for a 2.5% increase in ionic porosity.

Recent measurements indicate noble gases in amphiboles are located in the ring sites and that the solubility associated with the ring site is large compared to other minerals, such as olivine and pyroxene ([Heber et al., 2007](#); [Jackson et al., 2013b, 2015](#)). This implies that the porosity associated with an unoccupied ring site is fundamentally different compared to the remaining porosity within amphiboles in that noble gas atoms have an affinity for the porosity of the ring site, i.e. ring sites are relatively low energy locations for noble gases. The suggestion that not all porosity should be considered equal also draws support from correlations between He retentivity and alpha particle recoil damage to apatite and zircon lattices ([Shuster et al., 2006](#); [Guenther et al., 2013](#)). This correlation has been explained as the consequence of the relative affinity of He atoms for damaged locations within mineral lattices ([Shuster et al., 2006](#); [Shuster and Farley, 2009](#)) or increased tortuosity in anisotropic lattices ([Guenther et al., 2013](#)).

Despite the importance of ring site porosity for noble gas solubility in amphibole, its effects on noble gas diffusivity have not been systematically investigated. Here we test the effect of increasing the ring site porosity on He and Ne diffusion in amphibole. Arrhenius relationships are

derived for four different amphibole compositions with a wide range of ring site porosity using a step-heating approach. The results of these experiments show that He and Ne diffusion is uniformly slower in amphiboles with a high concentration of unoccupied rings, supporting the hypothesis that low energy locations within minerals act to increase their retentivity. This result is the opposite as predicted by the simple application of ionic porosity-diffusion models and provides insight into how alpha recoil damage affects mineral lattices.

2. METHODS

2.1. Starting materials

Gem-quality amphiboles were used as the starting materials for the diffusion experiments. Major element compositions were determined by electron microprobe analysis on polished grain mounts (Brown University, Cameca SX-100). Analytical parameters were as follows: 15 kV accelerating voltage, 10 nA beam current, and a 10 μm beam. The PAP correction was applied. All specimens were analyzed 50 times. The averages and standard deviations of those analyses are reported in [Table 1](#). Cation stoichiometry is calculated assuming a charge balance of 23 oxygens. Ring site occupancy is calculated by assigning all Ca to the M4 site. Sodium is partitioned to the M4 site to satisfy the requirement of two M4 cations per functional unit. The remaining Na and all K are partitioned to the ring site. Ring site occupancy is taken as the sum of Na and K cations partitioned to the ring site. Other large radius elements, such as Rb and Ba, may also enter the ring site, but these are trace elements and should not significantly affect the occupancy calculation. All specimens were studied for He and Ne solubility in [Jackson et al. \(2013a\)](#) and have been reanalyzed for their major element chemistry.

2.2. Helium and Neon diffusion experiments

To produce a spatially homogeneous distribution of ^3He and ^{21}Ne , amphibole crystals were irradiated with a beam of 220 MeV (incident energy) protons for a continuous 5 h period at the Francis H. Burr Proton Therapy Center at the Massachusetts General Hospital ([Shuster et al., 2004](#)). The samples were irradiated with a total fluence of $\sim 8.5 \times 10^{15}$ protons cm^{-2} . In a previous study, quartz samples irradiated with fluences of 0.2×10^{15} and 6.2×10^{15} protons cm^{-2} had similar diffusion kinetics of both He and Ne after each irradiation, suggesting that these fluences did not induce significant amounts of radiation damage in quartz ([Shuster and Farley, 2005a](#)). Although we cannot completely exclude the possibility that some damage in the amphiboles resulted from the proton irradiation, we assume that the proton energy and fluence used in the present study did not introduce an amount of crystal damage that would have significantly influenced noble gas diffusivity. Following irradiation, the amphibole crystals were gently crushed and the resulting grains were hand-picked for fragments that were as equi-dimensional as possible and of sufficient size for precise analysis. Images of the

Table 1
Major elements composition of amphiboles.

wt.%	Clear pargasite		Richterite	Tremolite	Green actinolite			
	Avg.	1 σ						
SiO ₂	47.45	0.18	56.76	0.17	57.30	0.18	54.22	0.23
Al ₂ O ₃	12.15	0.09	1.55	0.06	0.92	0.11	5.87	0.07
TiO ₂	0.11	0.01	0.15	0.01	0.08	0.01	0.24	0.01
MgO	21.67	0.14	23.92	0.12	22.77	0.18	22.59	0.11
FeO	0.23	0.03	0.09	0.02	2.85	0.18	0.05	0.02
MnO	0.01	0.02	0.03	0.02	0.08	0.03	0.11	0.03
CaO	11.81	0.05	7.58	0.05	12.74	0.07	13.08	0.07
Na ₂ O	3.75	0.14	5.29	0.14	0.62	0.08	0.62	0.05
K ₂ O	0.53	0.02	1.96	0.02	0.23	0.03	0.56	0.01
F	1.30	0.08	0.92	0.06	0.52	0.11	0.71	0.06
Cl	0.01	0.01	0.01	0.01	0.02	0.01	0.00	0.00
Total	99.02		98.27		98.11		98.05	
<i>Cation stoichiometry</i>								
Si	6.59	0.02	7.83	0.01	7.89	0.02	7.42	0.02
Al (IV)	1.41	0.02	0.17	0.01	0.11	0.02	0.58	0.02
Al (VI)	0.57	0.02	0.08	0.01	0.03	0.01	0.37	0.02
Ti	0.01	0.00	0.02	0.00	0.01	0.00	0.02	0.00
Mg	4.48	0.02	4.92	0.02	4.67	0.03	4.61	0.02
Fe ⁺²	0.03	0.00	0.01	0.00	0.33	0.02	0.01	0.00
Mn	0.00	0.00	0.00	0.00	0.01	0.00	0.01	0.00
Ca	1.76	0.01	1.12	0.01	1.88	0.01	1.92	0.01
Na (M4)	0.24	0.01	0.88	0.01	0.12	0.01	0.08	0.01
Na (ring)	0.77	0.04	0.53	0.04	0.04	0.02	0.09	0.02
K (ring)	0.09	0.00	0.34	0.00	0.04	0.00	0.10	0.00
Unoccupied (ring)	0.14	0.04	0.12	0.03	0.92	0.02	0.82	0.02

Notes: Cation stoichiometry calculated assuming charge balance of 23 O.

grains are included as [Supplementary Material](#). These aliquots were then loaded into Pt–Ir tubes in direct contact with a type-K thermocouple under ultra high vacuum. Samples were then incrementally heated using a feedback-controlled 150 W diode laser ($\lambda = 810 \pm 10$ nm) focused onto the packet through a sapphire viewport. The molar quantities of ³He and ²¹Ne released in each step-heating increment were quantified using a MAP215-50 mass spectrometer in the Noble Gas Thermochronometry Lab of Berkeley Geochronology Center. The incremental heating data and average grain size are reported in the [Supplementary Tables](#) for each analyzed phase. Step-degassing methods are described in detail in [Tremblay et al. \(2014\)](#).

2.3. Calculation of diffusion coefficients

For each degassing increment we calculate the diffusion coefficient (D) normalized to the square of the characteristic length scale (a^2) using the equations of [Crank \(1975\)](#) for spherical geometry following the algorithm of [Fechtig and Kalbitzer \(1966\)](#). Activation energies (E_a) and normalized frequency factors (D_0/a^2) are calculated from linear regressions of $\ln(D/a^2)$ against inverse absolute temperature for each gas-amphibole combination. By taking this approach, we assume a uniform distribution of noble gases prior to the step-degassing experiment. This assumption is well supported by previous studies of He and Ne diffusivity in apatite and quartz samples, and in cases where another naturally occurring isotope (e.g., ⁴He) was known independently to have a spatially uniform distribution ([Shuster and](#)

[Farley, 2005a](#) and [Shuster and Farley, 2005b](#)). Errors reported for fitted parameters are strictly associated with the regression statistics and are 1 σ . Absolute frequency factors were determined by multiplying D_0/a^2 by the square of the characteristic length scale. Characteristic length scales are calculated as the radius of a sphere with the same surface area/volume ratio as the analyzed grain. Results of the Arrhenius relationship fitting are presented in [Table 2](#).

Confidence limits on Arrhenius relationships are derived using a Monte-Carlo approach. Random values are chosen for each E_a and D_0 pair according to a normal distribution around the best-fit value after accounting for any covariance in parameter uncertainty using a Cholesky decomposition. The randomly chosen coefficients are then used to calculate an Arrhenius relationship over the given temperature interval. This process was repeated 100 times for each amphibole-gas combination. Confidence limits are then calculated as a function of temperature by taking the standard deviation (1 σ) of predicted diffusivities at each temperature.

3. RESULTS

Arrhenius relationships are shown for each amphibole-gas combination in [Figs. 1–4](#). Plots of fitting residuals versus cumulative release and the time–temperature path for step-degassing are given as subpanels (B) and (C) in [Figs. 1–4](#), respectively. Data selected for fitting Arrhenius relationships are highlighted by a circle about the data point marker (dot). The fitted data were chosen to maximize the number of continuous degassing increments that

Table 2
Diffusion parameters.

	³ He			²¹ Ne			D_0 $\log_{10}(\text{m}^2 \text{s}^{-1})$	$D_0 \ln(\text{s}^{-1})$	E_a (J mol ⁻¹)	1σ	Rad. (μm)	
	E_a (J mol ⁻¹)	1σ	D_0 $\log_{10}(\text{m}^2 \text{s}^{-1})$	1σ	$D_0 \ln(\text{s}^{-1})$	1σ						
Clear pargasite	1.13E+05	2.38E+03	6.47	0.41	-5.28	0.18	1.66E+05	3.44	6.95E+03	0.84	0.37	90
Richterite	1.21E+05	1.55E+03	5.56	0.25	-5.04	0.11	1.73E+05	3.66	8.53E+03	1.10	0.48	186
Tremolite	1.16E+05	1.40E+03	2.60	0.20	-6.38	0.09	1.39E+05	-3.37	5.84E+03	0.71	0.31	176
Green actinolite	1.01E+05	2.21E+03	0.56	0.31	-7.51	0.14	NR	NR	NR	NR	NR	132

Notes: NR – none reported; errors are 1σ ; rad. – characteristic length scale for diffusion.

precede clear departures from linear Arrhenius arrays at high temperature. The fits of He data include the large majority (>95%) of measured data points and gas analyzed. Neon fits are primarily based on mid-range temperature increments and significantly less of the total gas released (~10–40%). Higher temperatures are required to extract measurable quantities of Ne compared to He, and following this, ²¹Ne fits do not include the lowest temperature extractions used to regress the He data. Some low temperature increments do yield detectable ²¹Ne, but these quantities are small and do not display any clear correlation with temperature and are not used for fitting purposes. These lower temperature increments are likely affected by outgassing of relatively small radius domains (e.g., adhering dust), biasing D/a^2 to higher values. The highest temperature increments (>~1000 °C) are repeatedly associated with relatively large and irregular releases of ²¹Ne. These higher temperature increments, and any subsequent lower temperature increments, are not used for fitting purposes. Despite the lower fraction of analyzed gas for ²¹Ne compared to ³He, these fits incorporate a sufficient number of measurements and range in temperature to determine Arrhenius relationships (neglecting ²¹Ne release from green actinolite, discussed below). Data chosen for fitting were collected as consecutive degassing increments along the prescribed time–temperature path, neglecting a single data point associated with the release of Ne from the tremolite specimen. All degassing experiments also yielded reproducible D/a^2 values at multiple, isothermal steps for ³He and ²¹Ne. This reproducible behavior is consistent with a uniform distribution of ³He and ²¹Ne in the measured grains.

The ²¹Ne release pattern of the green actinolite specimen is erratic, precluding fitting an Arrhenius relationship with confidence. The exact reason for the erratic behavior is not clear as the ³He release from the same specimen is well behaved and overlaps in temperature with those associated with the erratic ²¹Ne releases. Nonetheless, it is clear that ²¹Ne diffusivity in the green actinolite at moderate temperatures is similar to those measured for the other unoccupied ring site-rich amphibole (tremolite) and distinctly lower than measured for occupied ring site-rich amphiboles (clear pargasite and richterite).

All Arrhenius relationships with corresponding confidence intervals are plotted in Fig. 5. These relationships are plotted as absolute diffusivity to facilitate inter-amphibole comparison and comparison with the Ar Arrhenius relationship reported by Harrison (1981). Helium is uniformly the most mobile in amphibole, followed by Ne and Ar. Activation energies increase from He to Ar, and the differences in diffusivity between amphiboles with majority occupied ring sites and majority unoccupied ring sites are similar for both He and Ne.

4. DISCUSSION

Our primary finding is that He and Ne diffusion is systematically slower in amphiboles with high concentrations of unoccupied ring sites compared to amphiboles with low concentrations of unoccupied ring sites (Fig. 5). This result is counterintuitive because amphiboles with higher

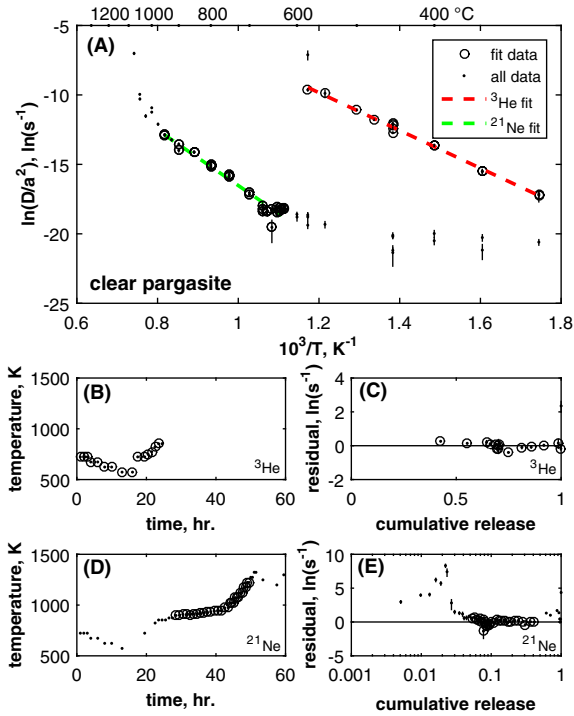


Fig. 1. Diffusion kinetics of ^3He and ^{21}Ne in clear pargasite. (A) Arrhenius plots of ^3He and ^{21}Ne releases. Fitted Arrhenius relationships for ^3He (red) and ^{21}Ne (green) are plotted as dashed lines. Dashed lines for regressions are used to denote amphiboles with the majority of their ring sites occupied. Dots represent increments that yielded detectable amounts of ^3He or ^{21}Ne . Circled dots represent increments used for fitting. (B) Time–temperature path of the ^3He outgassing experiment. (C) Residuals to the fitted ^3He Arrhenius relationship plotted as a function of the cumulative release fraction. (D) Time–temperature path of the ^{21}Ne outgassing experiment. (E) Residuals to the fitted ^{21}Ne Arrhenius relationship plotted as a function of the cumulative release fraction. Note the rescaling of x-axes between ^3He and ^{21}Ne plots in (C) and (E). Error bars are 1σ . (For interpretation of the references to colour in this figure legend, the reader is referred to the web version of this article.)

concentrations of unoccupied ring sites have higher ionic porosity. Ionic porosity correlates linearly with \log_{10} Ar diffusivity at a given temperature for a range of mineral types (Fortier and Giletti, 1989), such that, all other variables being constant, one would expect noble gases to diffuse more rapidly through an amphibole with a high concentration of unoccupied ring sites (Dahl, 1996). Our observation that He and Ne diffuse more slowly through amphiboles with unoccupied ring sites suggests that as noble gases migrate through the amphibole lattice and encounter a ring site, their mobility is effectively hindered, implying that ring sites, as high solubility features in amphibole, operate as traps for noble gases. This result is qualitatively consistent with modeling the effects of nano-scale pores on Ar diffusion in quartz, where higher Ar solubility in pores and higher pore concentrations act to progressively slow bulk Ar diffusion (Watson and Cherniak, 2003).

The observed magnitude of the ring site trapping effect is significant. Comparing the two amphiboles with the majority

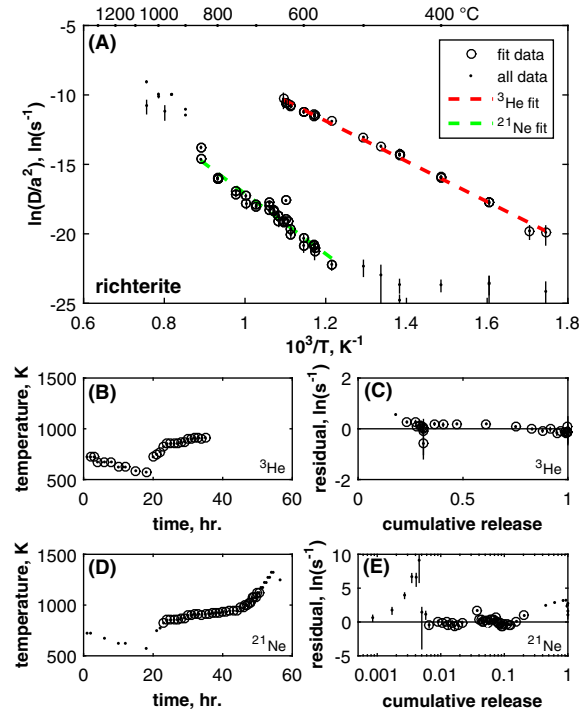


Fig. 2. Diffusion kinetics of ^3He and ^{21}Ne in richterite. All symbols and details as described in the caption of Fig. 1.

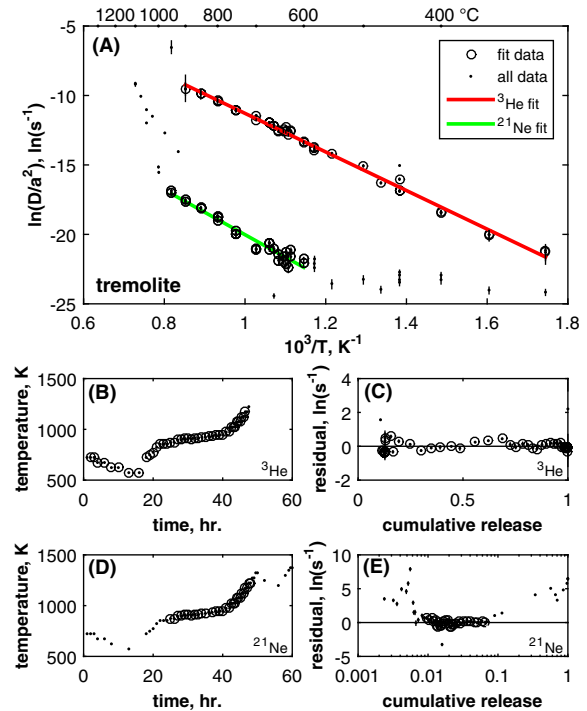


Fig. 3. Diffusion kinetics of ^3He and ^{21}Ne in actinolite. All symbols and details as described in the caption of Fig. 1. Solid lines for regressions are used to denote amphiboles with the majority of their ring sites unoccupied.

of their ring sites occupied to the two amphiboles with the majority of their ring sites unoccupied, we observe a 10–30 \times increase in He and Ne diffusivity at 500 and 700 $^{\circ}\text{C}$, respectively

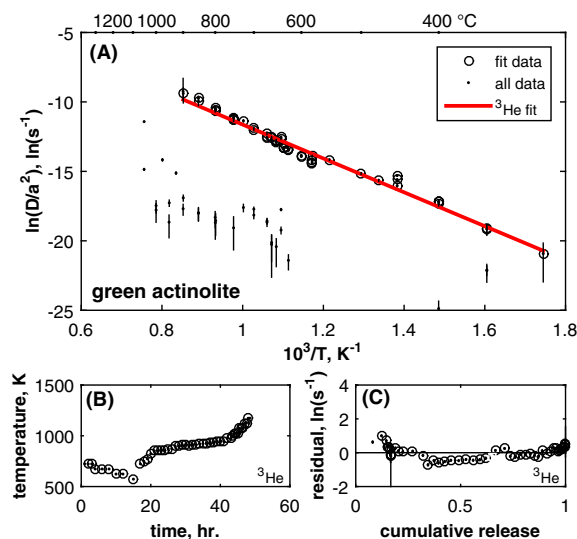


Fig. 4. Diffusion kinetics of ^3He and ^{21}Ne in green actinolite. All symbols and details as described in the caption of Fig. 1. Solid lines for regressions are used to denote amphiboles with the majority of their ring sites unoccupied. We do not report an Arrhenius relationship for the ^{21}Ne data because of the erratic release pattern. Despite the erratic ^{21}Ne release pattern, it is clear that Ne diffuses significantly slower than ^3He in the green actinolite specimen.

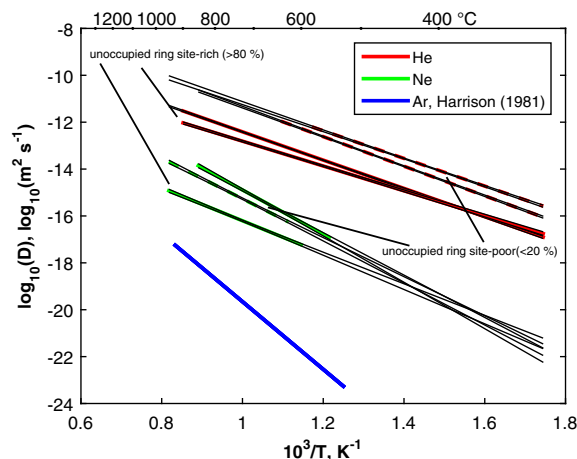


Fig. 5. Compilation of He, Ne and Ar Arrhenius relationships in amphiboles. Arrhenius relationships from this study and Harrison (1981) converted into absolute diffusivities using their characteristic length scales. Confidence limits are provided on reported data and are calculated using a Monte Carlo approach. Higher diffusivities are associated with smaller noble gases, and activation energies increase with noble gas radius. Between amphiboles with the majority of ring sites occupied (dashed lines) and unoccupied (solid lines) there is a clear offset of diffusivities for both He and Ne datasets, where higher diffusivities are associated with occupied ring sites. There is no systematic difference in E_a values when comparing amphiboles with the majority of ring sites occupied and unoccupied.

(dashed lines vs. dotted lines in Fig. 5). Increasing the D_0 value reported by Harrison (1981) for Ar diffusion in amphibole by $30\times$ lowers the corresponding T_c value by 74°C ($500\ \mu\text{m}$ grain cooling at $100^\circ\text{C Myr}^{-1}$; Dodson, 1973).

Experiments focused on He and Ne dissolution into amphibole highlight the importance of ring sites in controlling the solubility of noble gases (Jackson et al., 2013a, 2015). These results demonstrate the relative affinity of noble gases, as large radius, neutrally charged elements, for large radius, neutrally charged sites, such as the ring site. Interestingly, these experiments demonstrate that He is consistently more soluble than Ne in amphibole. The fact that He and Ne diffusion are similarly hindered by the presence of unoccupied ring sites suggests that the activation energies associated with He and Ne migrating from the ring site and into the activated state before migrating to an adjacent site are similar despite their differing solubility (Gautheron et al., 2009; Flowers et al., 2009).

4.1. *In vacuo* heating of amphibole

Previous efforts focused on understanding the behavior of amphibole during *in vacuo* heating have demonstrated that amphibole undergoes structural decomposition near 1000°C (Gaber et al., 1988; Lee et al., 1991; Wartho et al., 1991; Lee, 1993). The erratic release patterns at high temperatures are consistent with these previous studies, but it is worth noting that lower temperature data points collected following the high temperature increments tend to yield diffusivities similar to those collected during the prograde portion of the time–temperature path. *In vacuo* heating below 900°C is associated with H-loss and oxidation of Fe^{+2} but not structural changes (Gerling et al., 1966; Gaber et al., 1988; Lee et al., 1991; Wartho et al., 1991). The well-behaved nature of He releases across a wide range of temperatures ($300\text{--}900^\circ\text{C}$), particularly for green actinolite and tremolite, which retain He to high temperatures, argues strongly against H-loss or other effects at low temperature significantly affecting noble gas diffusion kinetics reported here. Moreover, our diffusion data for He in green actinolite and tremolite specimens (majority unoccupied ring sites) compare well with previous measurements of He diffusion in hornblende that extend to lower temperatures than those explored here (Lippolt and Weigel, 1988), and the amphiboles studied here have low Fe#, minimizing the amount of oxidative stress that can be generated.

4.2. Comparison to alpha particle recoil damage in apatite and zircon

The concept of low energy sites within minerals hindering noble gas mobility gains support from studies focused on the effect of alpha particle recoil damage on He mobility in apatite and zircon (Shuster et al., 2006; Shuster and Farley, 2009; Flowers et al., 2009; Guenther et al., 2013). Helium (^4He) is produced by alpha decay, most prominently along the U- and Th-series decay chains, and these decays cause lattice damage, such as zones that are depleted in atoms, mainly resulting from the recoil of the parent nuclide (e.g., Trachenko et al., 2002). It has been demonstrated that He diffusivity progressively decreases in apatite and zircon as the concentration of alpha particle recoil damage increases, taking $[\text{He}]$ as a proxy for recoil damage (Shuster et al., 2006; Guenther et al., 2013).

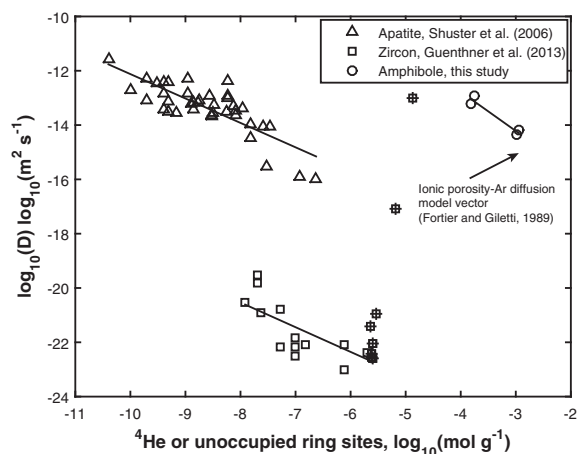


Fig. 6. Compilation He diffusion results for zircon, apatite, and amphibole plotted as a function of ^4He concentration (a proxy for alpha radiation damage density for apatite and zircon) or unoccupied ring site density (amphibole). Plotted diffusivities are calculated from reported Arrhenius relationships at a constant temperature. The temperatures selected for the zircon, apatite, and amphibole comparisons are 373, 473, and 773 K, respectively. These temperatures were selected to compare the minerals at temperatures where experimental data were collected and are robust; the comparisons are not sensitive to the chosen temperatures. Zircon data are plotted as a single group, irrespective of mineralogical orientation. The vector predicted by the ionic porosity model for the dependence of Ar diffusion on the concentration of unoccupied ring sites is also plotted for comparison (Fortier and Giletti, 1989).

Fig. 6 compares the rate of He diffusion at a given temperature to the concentration of ^4He in apatite and zircon and the concentration of unoccupied ring sites in amphibole. It is clear that alpha particle recoil damage and unoccupied ring site concentration both correlate with lower He diffusivity according to a power law relationship and that the slopes of the correlations are of similar magnitude. We also plot in Fig. 6 the vector predicted by the ionic porosity model for the dependence of Ar diffusion on the concentration of unoccupied ring sites (Fortier and Giletti, 1989). Our observations demonstrate that ionic porosity with relatively high associated noble gas solubility acts to slow, rather than hasten, noble gas diffusion (Watson and Cherniak, 2003). The concentration of unoccupied ring sites in amphibole is high, even compared to zircons with large accumulations of radiation damage. Guenther et al. (2013) observed a sharp increase in He diffusivity in zircon for samples with large accumulations of radiation damage, which they attributed to an interconnection of alpha particle recoil damage (Salje et al., 1999; Ketcham et al., 2013). The data associated with this regime in zircon are plotted as crossed box symbols in Fig. 6. Concerning amphibole, the lattice distribution of ring sites in amphibole ensures that they remain isolated from each other regardless of their overall concentration. If He diffusion is slowed by unoccupied ring sites, noble gas traps are potentially effective up to extreme concentrations, depending on their distribution and size.

The correlation between He diffusivity and unoccupied ring site concentration in amphibole supports the hypothesis that alpha decay events generate low energy traps in minerals (Shuster et al., 2006), at least in a proportion of decay events. In minerals with isotropic diffusive behavior, such as apatite, the generation of low energy sites may be the most significant consequence of low dose alpha radiation, whereas in minerals with anisotropic diffusive behavior, such as zircon, low energy site generation may compete with other effects (e.g., tortuosity; Guenther et al., 2013) in determining the net effect of alpha radiation.

4.3. Influence of ring site traps on noble gas recycling to Earth's mantle

Mounting evidence suggests that atmospheric noble gases, despite their geochemically inert behavior, are recycled into deep into subduction zones and ultimately into Earth's mantle (e.g., Nagao and Takahashi, 1993; Matsumoto et al., 2001; Holland and Ballentine, 2006; Sumino et al., 2010; Hopp and Ionov, 2011; Kendrick et al., 2011, 2013; Mukhopadhyay, 2012; Parai et al., 2012; Tucker et al., 2012; Peto et al., 2013; Parai and Mukhopadhyay, 2015). This evidence raises the possibility that noble gases can potentially serve as elementally and isotopically diverse tracers of volatile element exchange between Earth's exterior and interior. Development of these tracers will allow further insight into the origins of fluids that flux the mantle wedge and the time-integrated history of volatile recycling.

Experiments directed toward understanding the possible carrier phases responsible for recycling noble gases, however, remain relatively sparse (e.g., Zaikowski and Schaeffer, 1979; Podosek et al., 1981; Jackson et al., 2013a, 2015). Subducting slabs represent the primary flux of mass from Earth's surface to interior, leading to the hypothesis that atmospheric noble gases initially present in slab materials are at least partially retained during the subduction process, despite massive fluid loss to the forearc and overlying mantle wedge (e.g. Moore and Vrolijk, 1992; Schmidt and Poli, 1998). The ability of a phase within a subducting slab to recycle noble gases is related to its affinity for and retentivity of noble gases, where higher solubility and lower diffusivity favor recycling over release.

Amphibole is a common phase in altered oceanic crust and is stable in subducting slabs to ~ 3 GPa or ~ 100 km depth (Ito et al., 1983; Schmidt and Poli, 1998; Carlson, 2003). Furthermore, noble gases are relatively soluble in amphibole (Jackson et al., 2013a, 2015), and amphibole is also anomalously retentive of Ar, and by extension Kr and Xe, compared to other common crustal minerals. The Ar T_c value for amphibole is 600°C ($500\ \mu\text{m}$ grain cooling at $100^\circ\text{C Myr}^{-1}$; Dodson, 1973). Muscovite, biotite, and plagioclase have T_c values that are ~ 50 , ~ 300 , and $\sim 400^\circ\text{C}$ lower than amphibole for equivalent conditions (see Baxter, 2010 for a compilation). It is likely that the high T_c value associated with amphibole reflects, at least to a degree the trapping effects of ring sites. Taken together, these T_c determinations suggest that amphibole is a potentially important carrier phase of noble gases during

subduction, further supported by the fact that amphiboles stabilized in subducting crust tend to be rich in unoccupied ring sites (e.g., glaucophane), further enhancing noble gas solubility and retentivity. These properties of amphibole warrant its study as an endmember case for noble gas transport by minerals in subduction zones.

We can estimate the net effect of ring site occupancy on Ne retention in an amphibole-rich region of a subducting slab by combining our experimental observations with a 1-D diffusion model. We model Ne loss using the mean value of diffusive parameters for richterite and clear pargasite (Table 2; unoccupied ring site-poor) and compare the results to a hypothetical unoccupied ring site-rich amphibole with a D_0 value that is $30\times$ higher, more analogous to amphibole in subducting slabs. For this calculation, we do not compare tremolite to richterite or clear pargasite because they have differing values of E_a , which complicates the comparison and obscures the isolated effect of ring site occupancy. Increasing the concentration of traps in a mineral should act to increase the activation energy for diffusion so long as the traps are not interconnected (Shuster et al., 2006), making the diffusive offsets we observe at high temperatures lower limits for lower temperature scenarios. We note that there is no clear offset of E_a values between amphiboles with high and low concentrations of unoccupied ring sites. Our model calculates the diffusive loss of Ne initially hosted in a cylindrical amphibole grain

(200 μm radius) that is subjected to an intermediate subduction zone geotherm (S. Philippines, descent rate = 62 km Ma^{-1} , Syracuse et al., 2010) using the kinetic parameters described above. We do not account for any dissolution-precipitation processes affecting the size or concentration of noble gases in the modeled amphibole.

The system comprises an amphibole grain surrounded by an effectively infinite porosity that serves as a sink for noble gases. By assuming a large porosity surrounding amphibole, we isolate the role of diffusion in controlling noble gas exchange with its environment. Smaller amounts of porosity allow significant Ne fugacity build in the fluid, which acts to limit the loss of Ne from minerals according to their solubility (Baxter, 2003; Smye et al., 2013). Any Ne that is partitioned into the fluid has the potential to be lost from the slab, depending on the fluid mobility.

The results of this modeling are presented in Fig. 7. Black lines correspond to scenarios for amphiboles that are located at the MOHO of the subducting oceanic lithosphere, and gray lines correspond to scenarios for amphiboles that are located in the extrusive layer of oceanic crust. Together, these bracket the potential geotherms that a crustal amphibole would experience during subduction of the S. Philippines plate. Increasing D_0 of Ne by $30\times$ extends the point of initial Ne release deeper by $\sim 10 \text{ km}$ for the extrusive scenarios and by $\sim 20 \text{ km}$ for the MOHO scenarios. Following the point of initial release, all scenarios

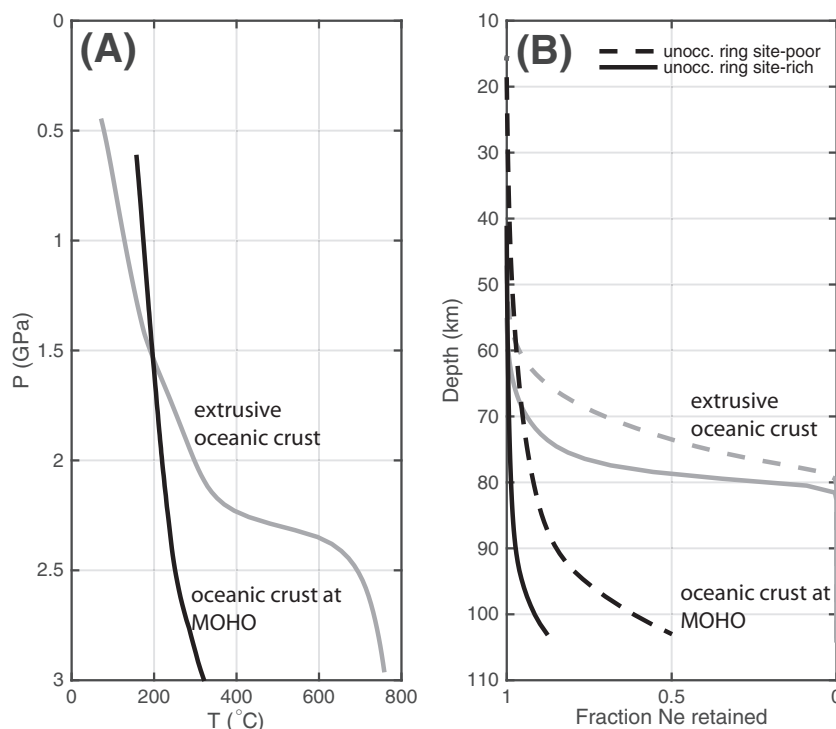


Fig. 7. Implications of Ne diffusion kinetics to modeling Ne extraction of amphibole-bearing oceanic crust during subduction. (A) Pressure-temperature path of oceanic crust during subduction of S. Philippines plate from Syracuse et al. (2010). The extrusive sections of oceanic crust experience a sharp increase in temperature upon coupling with the mantle wedge (gray line). Oceanic crust at the MOHO (black line) remains relatively cool up to the maximum pressures associated with amphibole stability. (B) Neon becomes mobile in extrusive sections of oceanic crust regardless of the availability of unoccupied ring sites once the mantle wedge is encountered. At the MOHO, temperatures remain cool enough that significant amounts of Ne can be retained. Here, unoccupied ring sites (solid black line) have the potential to significantly affect the efficiency of Ne recycling.

experience a zone of partial retention. For the extrusive scenarios (gray lines), the depth interval of partial retention is relatively narrow, reflecting the rapid increase in temperature experienced by the upper regions of the slab as it couples with the mantle wedge. Both amphibole compositional groups in the extrusive scenarios effectively experience complete Ne extraction at similar depths (~80 km), or equivalently, pressures (2.2 GPa). Amphiboles are particularly retentive of noble gases compared to other crustal minerals, suggesting that the Ne initially hosted by other mineral phases in the extrusive section of oceanic crust will be lost to fluids at depths shallower than those modeled here. Thus, while the compositional effects on Ne diffusion in amphibole are large, in all extrusive scenarios Ne becomes sufficiently mobile to afford complete extraction from the upper regions of a subducting slab by a migrating fluid phase at relatively shallow pressures. Heavier noble gases, Ar, Kr, and Xe, will diffuse slower than Ne and be less easily extracted along the same geotherm, providing a mechanism for preferentially recycling heavier noble gases and fluxing the mantle with fluids enriched in lighter noble gases. The implications of such a mechanism for noble gas systematics will be explored in a sister manuscript.

More deeply seated amphiboles (black lines) are thermally insulated from the mantle wedge, and consequently, experience a much smaller increase in temperature during subduction. This lower temperature geotherm allows amphibole to retain significant quantities of Ne to the maximum pressures associated with amphibole stability (3.0 GPa; [Forneris and Holloway, 2003](#)). Unoccupied ring site-poor amphiboles still experience ~50% extraction of their initial Ne, despite the thermal insulation provided by oceanic crust. Again, this implies a high mobility of Ne in other, less retentive phases also located deeper in the oceanic crust. Unoccupied ring site-rich amphiboles retain the large majority of their initial Ne, demonstrating that the increased retentivity associated with ring site traps has the potential to significantly enhance the efficiency of Ne recycling in cooler sections of subducting oceanic crust. Taken together, this suggests that amphibole can transport noble gases (Ne–Xe) to and potentially past depths of arc magma genesis (120 ± 40 km; [Tatsumi, 2005](#)). Further investigation is required to understand the fate of amphibole-born noble gases at pressures exceeding the amphibole stability field.

We focus here on Ne because of its potential to be recycled and the scope of the reported data. Helium is lost from Earth's atmosphere and is extremely mobile, severely limiting its concentration in subducted slab materials. Our data do not extend to heavier noble gases (Ar–Xe), but given the fact that both He and Ne are similarly affected by unoccupied ring sites, it is likely that the model applies to the heavier noble gases as well, i.e. unoccupied ring site-rich amphiboles enhance noble gas recycling efficiency in general. We note that where amphibole is scarce or where other high noble gas solubility phases are present in slabs, amphibole will not control the bulk lithology behavior for noble gases. Nonetheless, the general modeling approach taken here can be extended to other minerals provided the appropriate noble gas solubility and diffusivity data are available.

5. CONCLUSIONS

We report measurements of He and Ne diffusivity for a set of amphiboles with a large range of unoccupied ring site concentrations. These results demonstrate that low energy sites within amphibole act to hinder the diffusive mobility of He and Ne. Furthermore, this finding confirms that gross ionic porosity, alone, cannot account for the diffusion systematics of noble gases in amphibole. A comparison of amphibole, zircon, and apatite indicates that greater densities of alpha particle recoil damage and unoccupied ring sites each correlate with lower He diffusivity, and with similar relationships despite the different manifestation of noble gas “traps” in these minerals. Application of the observed diffusion systematics to a subduction model for oceanic crust suggests the following: (1) Ne is sufficiently mobile to be efficiently extracted from all amphiboles in the upper-most sections of subducted crust and (2) along cooler geothermal gradients associated with the lower-most oceanic crust, unoccupied ring site-rich amphiboles are substantially more retentive of Ne compared to unoccupied ring site-poor amphiboles, allowing for near-complete retention of Ne up to the maximum stability of amphibole. As Ne is a relatively mobile noble gas, this later result implies that large fractions of heavier noble gases can be retained in lower oceanic crust as well. More generally, our results suggest that the topology of ionic porosity competes with the absolute volume of ionic porosity in controlling the rate of noble gas diffusion in minerals.

ACKNOWLEDGEMENTS

Pete Burnard handled this manuscript as the AE before his sudden death. We wish to acknowledge his diverse contributions to noble gas geochemistry as an experimentalist, analyst, and editor. His wit and enthusiasm are missed. We thank Marc Norman for handling this manuscript following the review stage. Ethan Baxter and an anonymous reviewer helped to improve the manuscript. We additionally thank Nicholas Fylstra for his help with the outgassing experiments, Jack Krantz and Joe Boesenberg for their help with the electron microprobe measurements, and Willy Guenther for sharing his compilation of zircon outgassing data. Discussions with Reid Cooper helped in developing the noble gas distribution in slab model. D.L.S. acknowledges support from the Ann and Gordon Getty Foundation. S.W.P. acknowledges support from NSF-EAR 1347772. CRMJ acknowledges Carnegie Institute of Washington for fellowship support.

APPENDIX A. SUPPLEMENTARY DATA

Supplementary data associated with this article can be found, in the online version, at <http://dx.doi.org/10.1016/j.gca.2015.09.024>.

REFERENCES

- Baxter E. F. (2003) Quantification of the factors controlling the presence of excess ^{40}Ar or ^4He . *Earth Planet. Sci. Lett.* **216**, 619–634.
- Baxter E. F. (2010) Diffusion of noble gases in minerals. *Rev. Mineral. Geochem.* **72**, 509–557.

- Berry R. F. and McDougall I. (1986) Interpretation of $^{40}\text{Ar}/^{39}\text{Ar}$ and K/Ar dating evidence from the Aileu Formation, East Timor, Indonesia. *Chem. Geol. Isotope Geosci. Section* **59**, 43–58.
- Carlson R. L. (2003) Bound water content of the lower oceanic crust estimated from modal analyses and seismic velocities of oceanic diabase and gabbro. *Geophys. Res. Lett.* **30**, 2142.
- Crank J. (1975) *The Mathematics of Diffusion*. Clarendon press, Oxford.
- Dahl P. S. (1996) The effects of composition on retentivity of argon and oxygen in hornblende and related amphiboles: a field-tested empirical model. *Geochim. Cosmochim. Acta* **60**, 3687–3700.
- Dodson M. H. (1973) Closure temperature in cooling geochronological and petrological systems. *Contrib. Miner. Petrol.* **40**, 259–274.
- Dowty E. (1980) Crystal-chemical factors affecting the mobility of ions in minerals. *Am. Mineral.* **65**, 174–182.
- Fechtig H. and Kalbitzer S. (1966) The diffusion of argon in potassium-bearing solids. In *Potassium Argon Dating*. Springer, pp. 68–107.
- Flowers R. M., Ketcham R. A., Shuster D. L. and Farley K. A. (2009) Apatite (U–Th)/He thermochronometry using a radiation damage accumulation and annealing model. *Geochim. Cosmochim. Acta* **73**, 2347–2365.
- Forneris J. F. and Holloway J. R. (2003) Phase equilibria in subducting basaltic crust: implications for H_2O release from the slab. *Earth Planet. Sci. Lett.* **214**, 187–201.
- Fortier S. M. and Giletti B. J. (1989) An empirical model for predicting diffusion coefficients in silicate minerals. *Science* **245**, 1481–1484.
- Gaber L. J., Foland K. A. and Corbató C. E. (1988) On the significance of argon release from biotite and amphibole during $^{40}\text{Ar}/^{39}\text{Ar}$ vacuum heating. *Geochim. Cosmochim. Acta* **52**, 2457–2465.
- Gautheron C., Tassan-Got L., Barbarand J. and Pagel M. (2009) Effect of alpha-damage annealing on apatite (U–Th)/He thermochronology. *Chem. Geol.* **266**, 157–170.
- Gerling E., Petrov B. and Koltsova T. (1966) A comparative study of the activation energy of argon liberation and dehydration energy in amphiboles and biotites. *Geochem. Int.* **3**, 295–305.
- Guenther W. R., Reiners P. W., Ketcham R. A., Nasdala L. and Giester G. (2013) Helium diffusion in natural zircon: radiation damage, anisotropy, and the interpretation of zircon (U–Th)/He thermochronology. *Am. J. Sci.* **313**, 145–198.
- Hacker B. R. and Wang Q. (1995) Ar/Ar geochronology of ultrahigh-pressure metamorphism in central China. *Tectonics* **14**, 994–1006.
- Harrison T. M. (1981) Diffusion of ^{40}Ar in hornblende. *Contrib. Miner. Petrol.* **78**, 324–331.
- Harrison T. M. and Fitzgerald J. D. (1986) Exsolution in hornblende and its consequences for $^{40}\text{Ar}/^{39}\text{Ar}$ age spectra and closure temperature. *Geochim. Cosmochim. Acta* **50**, 247–253.
- Harrison T. M. and McDougall I. (1980) Investigations of an intrusive contact, northwest Nelson, New Zealand—II. Diffusion of radiogenic and excess ^{40}Ar in hornblende revealed by $^{40}\text{Ar}/^{39}\text{Ar}$ age spectrum analysis. *Geochim. Cosmochim. Acta* **44**, 2005–2020.
- Heber V. S., Brooker R. A., Kelley S. P. and Wood B. J. (2007) Crystal-melt partitioning of noble gases (helium, neon, argon, krypton, and xenon) for olivine and clinopyroxene. *Geochim. Cosmochim. Acta* **71**, 1041–1061.
- Holland G. and Ballentine C. J. (2006) Seawater subduction controls the heavy noble gas composition of the mantle. *Nature* **441**, 186–191.
- Hopp J. and Ionov D. A. (2011) Tracing partial melting and subduction-related metasomatism in the Kamchatkan mantle wedge using noble gas compositions. *Earth Planet. Sci. Lett.* **302**, 121–131.
- Ito E., Harris D. M. and Anderson A. T. (1983) Alteration of oceanic crust and geologic cycling of chlorine and water. *Geochim. Cosmochim. Acta* **47**, 1613–1624.
- Jackson C. R. M., Parman S., Kelley S. P. and Cooper R. F. (2013a) Noble gas transport into the mantle facilitated by high solubility in amphibole. *Nat. Geosci.* **6**, 562–565.
- Jackson C. R. M., Parman S. W., Kelley S. P. and Cooper R. F. (2013b) Constraints on light noble gas partitioning at the conditions of spinel-peridotite melting. *Earth Planet. Sci. Lett.* **384**, 178–187.
- Jackson C. R. M., Parman S. W., Kelley S. P. and Cooper R. F. (2015) Light noble gas dissolution into ring structure-bearing materials and lattice influences on noble gas recycling. *Geochim. Cosmochim. Acta* **159**, 1–15.
- Kendrick M. A., Honda M., Pettke T., Scambelluri M., Phillips D. and Giuliani A. (2013) Subduction zone fluxes of halogens and noble gases in seafloor and forearc serpentinites. *Earth Planet. Sci. Lett.* **365**, 86–96.
- Kendrick M. A., Scambelluri M., Honda M. and Phillips D. (2011) High abundances of noble gas and chlorine delivered to the mantle by serpentinite subduction. *Nat. Geosci.* **4**, 807–812.
- Ketcham R. A., Guenther W. R. and Reiners P. W. (2013) Geometric analysis of radiation damage connectivity in zircon, and its implications for helium diffusion. *Am. Mineral.* **98**, 350–360.
- Lee J. K. W. (1993) The argon release mechanisms of hornblende in vacuo. *Chem. Geol.* **106**, 133–170.
- Lee J. K. W., Onstott T. C., Cashman K. V., Cumbest R. J. and Johnson D. (1991) Incremental heating of hornblende in vacuo: implications for $^{40}\text{Ar}/^{39}\text{Ar}$ geochronology and the interpretation of thermal histories. *Geology* **19**, 872–876.
- Lippolt H. J. and Weigel E. (1988) ^4He diffusion in ^{40}Ar retentive minerals. *Geochim. Cosmochim. Acta* **52**, 1449–1458.
- Matsumoto T., Chen Y. and Matsuda J.-I. (2001) Concomitant occurrence of primordial and recycled noble gases in the Earth's mantle. *Earth Planet. Sci. Lett.* **185**, 35–47.
- Moore J. C. and Vrolijk P. (1992) Fluids in accretionary prisms. *Rev. Geophys.* **30**, 113–135.
- Mukhopadhyay S. (2012) Early differentiation and volatile accretion recorded in deep-mantle neon and xenon. *Nature* **486**, 101–104.
- Nagao K. and Takahashi E. (1993) Noble gases in the mantle wedge and lower crust: an inference from the isotopic analyses of xenoliths from Oki-Dogo and Ichinomegata, Japan. *Geochem. J.* **27**, 229–240.
- O'Nions R. K., Smith D. G. W., Baadscaard H. and Morton R. D. (1969) Influence of chemical composition on argon retentivity in metamorphic calcic amphiboles from South Norway. *Earth Planet. Sci. Lett.* **5**, 339–345.
- Onstott T. C. and Peacock M. W. (1987) Argon retentivity of hornblendes: a field experiment in a slowly cooled metamorphic terrane. *Geochim. Cosmochim. Acta* **51**, 2891–2903.
- Parai R., Mukhopadhyay S. and Standish J. (2012) Heterogeneous upper mantle Ne, Ar and Xe isotopic compositions and a possible Dupal noble gas signature recorded in basalts from the Southwest Indian Ridge. *Earth Planet. Sci. Lett.* **359**, 227–239.
- Parai R. and Mukhopadhyay S. (2015) The evolution of MORB and plume mantle volatile budgets: constraints from fission Xe isotopes in Southwest Indian Ridge basalts. *Geochem. Geophys. Geosyst.* **16**, 719–735.
- Peto M. K., Mukhopadhyay S. and Kelley K. A. (2013) Heterogeneities from the first 100 million years recorded in deep mantle noble gases from the Northern Lau Back-arc Basin. *Earth Planet. Sci. Lett.* **369**, 13–23.

- Podosek F. A., Bernatowicz T. J. and Kramer F. E. (1981) Adsorption of xenon and krypton on shales. *Geochim. Cosmochim. Acta* **45**, 2401–2415.
- Salje E., Chrosch J. and Ewing R. (1999) Is “metamictization” of zircon a phase transition? *Am. Mineral.* **84**, 1107–1116.
- Schmidt M. W. and Poli S. (1998) Experimentally based water budgets for dehydrating slabs and consequences for arc magma generation. *Earth Planet. Sci. Lett.* **163**, 361–379.
- Shuster D. L., Farley K. A., Sistierson J. M. and Burnett D. S. (2004) Quantifying the diffusion kinetics and spatial distributions of radiogenic He-4 in minerals containing proton-induced He-3. *Earth Planet. Sci. Lett.* **217**, 19–32.
- Shuster D. L. and Farley K. A. (2005a) Diffusion kinetics of proton-induced ^{21}Ne , ^3He , and ^4He in quartz. *Geochim. Cosmochim. Acta* **69**, 2349–2359.
- Shuster D. L. and Farley K. A. (2005b) $^4\text{He}/^3\text{He}$ thermochronometry: theory, practice, and potential complications. *Rev. Mineral. Geochem.* **58**, 181–203.
- Shuster D. L., Flowers R. M. and Farley K. A. (2006) The influence of natural radiation damage on helium diffusion kinetics in apatite. *Earth Planet. Sci. Lett.* **249**, 148–161.
- Shuster D. L. and Farley K. A. (2009) The influence of artificial radiation damage and thermal annealing on helium diffusion kinetics in apatite. *Geochim. Cosmochim. Acta* **73**, 183–196.
- Smye A. J., Warren C. J. and Bickle M. J. (2013) The signature of devolatilisation: extraneous ^{40}Ar systematics in high-pressure metamorphic rocks. *Geochim. Cosmochim. Acta* **113**, 94–112.
- Sumino H., Burgess R., Mizukami T., Wallis S. R., Holland G. and Ballentine C. J. (2010) Seawater-derived noble gases and halogens preserved in exhumed mantle wedge peridotite. *Earth Planet. Sci. Lett.* **294**, 163–172.
- Syracuse E. M., van Keken P. E. and Abers G. A. (2010) The global range of subduction zone thermal models. *Phys. Earth Planet. Inter.* **183**, 73–90.
- Tatsumi Y. (2005) The subduction factory: how it operates in the evolving Earth. *GSA Today* **15**, 4.
- Trachenko K., Dove M. T. and Salje E. K. H. (2002) Structural changes in zircon under α -decay irradiation. *Phys. Rev. B* **65**, 180102.
- Tremblay M. M., Shuster D. L. and Balco G. (2014) Diffusion kinetics of ^3He and ^{21}Ne in quartz and implications for cosmogenic noble gas paleothermometry. *Geochim. Cosmochim. Acta* **142**, 186–204.
- Tucker J. M., Mukhopadhyay S. and Schilling J. G. (2012) The heavy noble gas composition of the depleted MORB mantle (DMM) and its implications for the preservation of heterogeneities in the mantle. *Earth Planet. Sci. Lett.* **355**, 244–254.
- von Blanckenburg F. and Villa I. M. (1988) Argon retentivity and argon excess in amphiboles from garbenschists of the western tauern window, eastern alps. *Contrib. Miner. Petrol.* **100**, 1–11.
- Wartho J., Dodson M., Rex D. and Guise P. (1991) Mechanisms of argon release from Himalayan metamorphic amphiboles. *Am. Mineral.* **59**, 121–127.
- Watson E. B. and Cherniak D. J. (2003) Lattice diffusion of Ar in quartz, with constraints on Ar solubility and evidence of nanopores. *Geochim. Cosmochim. Acta* **67**, 2043–2062.
- Zaikowski A. and Schaeffer O. A. (1979) Solubility of noble gases in serpentine: implications for meteoritic noble gas abundances. *Earth Planet. Sci. Lett.* **45**, 141–154.
- Zeitler P. K. (1985) Cooling history of the NW Himalaya, Pakistan. *Tectonics* **4**, 127–151.

Associate editor: Marc Norman